Research Square

Preprints are preliminary reports that have not undergone peer review.
They should not be considered conclusive, used to inform clinical practice,
or referenced by the media as validated information.

Effect of Curcumin-silver nanoparticles on proliferation of human lung squamous cell carcinoma(HTB182) and Pulmonary cell(HBE)

Wei Su

ssswww13@163.com

Hunan University of Technology

Bai Lin Dai

Hunan University of Technology

Li Tang

Hunan University of Technology

Li Bo Nie

Hunan University of Technology

Jian Xin Tang

Hunan University of Technology

Research Article

Keywords: Curcumin-AgNP, Human bronchial epithelial (HBE) cells, Human lung cancer (HTB-182) cells

Posted Date: May 18th, 2026

DOI: https://doi.org/10.21203/rs.3.rs-9535711/v1

License: This work is licensed under a Creative Commons Attribution 4.0 International License. Read Full License

Additional Declarations: No competing interests reported.

Abstract

Stable silver nanoparticles (AgNPs) were synthesized in vitro via the reaction of aqueous silver nitrate ($AgNO_3$) with water-soluble polymeric curcumin. Transmission electron microscopy (TEM) was employed to characterize the as-prepared AgNPs. TEM images revealed a distinct surface layer surrounding the AgNPs, with particle sizes ranging from 10 to 35 nm.The cytotoxicity of AgNPs against HTB-182 lung cancer cells and normal human bronchial epithelial (HBE) cells was evaluated at concentrations of 2, 4, 8, 10, 20, 30, 40, and 50 ppm using the Cell Counting Kit-8 (CCK-8) assay and optical microscopy. The results demonstrated that AgNP toxicity was dose-dependent in both HTB-182 and normal HBE cells, with a more pronounced cytotoxic effect observed in cancer cells.The half-maximal inhibitory concentration (IC_{50}) values of curcumin-AgNPs and silver ions were determined as follows: 15.6 ppm and 5.5 ppm for HBE cells, and 17.6 ppm and 11.3 ppm for HTB-182 cells, respectively. Subsequently, flow cytometry was used to investigate the effects of AgNPs and silver ions on apoptosis and cell cycle distribution in HTB-182 and HBE cells.Findings indicated that surface modification of AgNPs significantly influenced their anticancer and antiproliferative activities. Treatment with AgNPs or silver ions induced G0/G1 phase arrest in normal HBE cells, whereas HTB-182 non-small cell lung cancer cells exhibited G2/M phase arrest, likely attributable to DNA damage. These observations suggest that the cytotoxic mechanisms of silver ions and AgNPs differ between normal HBE cells and lung cancer cells.

1. Introduction

Lung cancer remains the leading cause of malignancy-related mortality worldwide, with more than one million new cases diagnosed annually. Non-small cell lung cancer (NSCLC) constitutes over 80% of all lung cancer diagnoses. According to the World Health Organization, the 5-year survival rate of lung cancer is merely 15%. Owing to the growing prevalence of smoking and persistent environmental degradation, the incidence of lung cancer has exhibited a progressive upward trend. To address this global challenge, the development and design of novel strategies, tools, and therapeutic agents for cancer diagnosis and treatment are urgently required.With advances in scientific research, nanomaterials have been recognized to not only optimize the physicochemical properties of pharmaceutical formulations but also enhance drug targeting and controlled release characteristics. Nanotechnology provides a promising approach for tumor targeting, acting either as a direct cytotoxic agent to eliminate tumor cells by disrupting cellular physiological functions or as delivery vehicles for specific therapeutic molecules[1].Silver nanoparticles (AgNPs) have been extensively explored in biomedical applications[2] owing to their facile synthesis[3–5], reliable quality control[6–8], and favorable biocompatibility. To date, AgNPs have been implemented in clinical settings, particularly for wound healing, owing to their potent antibacterial activity[9–14].The antitumor efficacy of AgNPs against lung cancer cell lines has been widely documented in recent studies, as summarized in Table 1[15–29]. According to previous investigations, AgNPs exhibit several distinctive advantages as potential anticancer candidates: their effective antitumor concentrations are relatively low, typically at the microgram-per-milliliter level; AgNPs display low systemic toxicity, with few reports of acute nanosilver-related toxicity; unlike organic chemotherapeutics, AgNPs are inorganic agents and exert more durable effects within tumor tissues. Furthermore, multiple studies have demonstrated that the inhibitory effects of AgNPs are significantly more pronounced in tumor cells than in normal cells.

Table 1
Anti-lung cancer effect of AgNPs

Application	Cells	Surface stability	Dose	Normal cells	Refs
Anti-lung cancer	**A549**	**PVP-AgNPs**	**0–20 mg/mL**	**None**	[15]
	H157	**Capped with sugar**	**IC_{50}: 3.6 mM**	**None**	[16]
	A549	**Tri-sodium citrate,**	**IC_{50}: 100 µg/mL**	**None**	[17, 18]
	A549	**Albizia adianthifolia**	**73% (50 µg/mL)**	**(PLs)**	[19]
	NCI-H460	**Chitosan-coated silver**	**IC_{50}: 2 µg/mL**	**(HEK)**	[20]
	A549	**Euphorbia nivulia**	**IC_{50}: 20 mgmL**	**None**	[21]
	A549	**Origanum vulgare**	**LD_{50}: 100 µg/mL**	**None**	[22]
	A549	**Rosa damascena petals**	**IC_{50}: 80 µg/mL**	**None**	[23]
	A549	**AgNP Cat. No. 576832**	**IC_{50}: 100–200 µg/mL**	**None**	[24]
	A549	**Micronized zeolite**	**LC_{50}: 4.1 µM**	**None**	[25]
	A549	**Poly-L-lysine (PLL)**		**None**	[26]
	A549	**PlasmaChem (Berlin)**	**2.5, 25, 100 µg/mL**	**None**	[27]
	A549	**Cymodocea serrulata**	**LD_{50}: 100 µg/mL**	**None**	[28]
	A549	**PAMAM and 5-FU**	**IC_{50}: 5 µg/mL**	**None**	[29]

However, numerous studies have been restricted to lung adenocarcinoma cell lines, such as A549, NCI-H460, and NCI-H157 cells. Investigations focusing on the anticancer activity of nanosilver against lung squamous cell carcinoma (LSCC) remain severely lacking. Compared with lung adenocarcinoma, lung squamous cell carcinoma is associated with an even poorer prognosis, with a 5-year patient survival rate of only 5%. Chemotherapy and molecular targeted therapy represent the current clinical strategies for locally advanced and metastatic lung squamous cell carcinoma.

Cytotoxic agents constitute the standard treatment for advanced lung squamous cell carcinoma. Common chemotherapy regimens include cisplatin combined with docetaxel or gemcitabine. Four third-generation chemotherapeutic drugs, namely paclitaxel, gemcitabine, vinorelbine, and docetaxel, plus platinum-based compounds are widely used as first-line treatments for advanced non-small cell lung cancer (NSCLC). The 1-year survival rate remains only 31–35%, and the efficacy of platinum-based chemotherapy has reached a therapeutic plateau.Pemetrexed is a preferred therapeutic option for advanced non-squamous NSCLC, yet it shows no clinical benefit in patients with squamous cell carcinoma. Regarding molecular targeted therapy for lung squamous cell carcinoma, the EGFR mutation rate is extremely low and lacks clear predictive value. Consequently, targeted therapy for lung squamous cell carcinoma has achieved no substantial breakthroughs or clinical improvements.Therefore, the development of novel therapeutic agents for lung squamous cell carcinoma is urgently needed. The aim of the present study was to develop an antitumor agent with low toxicity toward normal cells and potent inhibitory activity against target lung cancer cells, especially lung squamous cell carcinoma.

Curcumin is a phenolic pigment isolated from the rhizomes of Curcuma longa (genus Curcuma). Accumulating studies have demonstrated that curcumin exhibits diverse biological activities, including anti-inflammatory, antioxidant, and antitumor effects [30]. Curcumin is inexpensive and associated with exceptionally low toxicity. At present, research on its antitumor properties has mainly focused on cancer chemoprevention. Recently, the National Cancer Institute (NCI) of the United States has classified curcumin as a third-generation anticancer agent under clinical investigation.Several reports have indicated that curcumin exerts significant inhibitory effects against lung cancer. For instance, El Khoury et al. [31] reported that curcumin may suppress the growth and angiogenesis of A549 xenografts in nude mice. Lin et al. [32] demonstrated that curcumin exerts a radiosensitizing

effect on lung cancer cells, a finding further supported by Cai [33]. Similar observations have been documented by Wang[34] and Liu[35].

In the present study, curcumin-modified silver nanoparticles (curcumin-AgNPs) were synthesized at room temperature. Their apoptotic effects on normal HBE and HTB-182 lung squamous carcinoma cells were subsequently investigated using CCK-8 assays and flow cytometry. The results revealed that the antitumor and anticancer activities of silver nanoparticles are strongly influenced by surface modification. Accordingly, our findings provide a promising selective strategy for the treatment of lung squamous cell carcinoma, suggesting that curcumin-functionalized AgNPs hold potential as effective anticancer agents for clinical applications.Furthermore, the underlying mechanism by which curcumin-conjugated silver nanocrystals regulate cellular function was explored via cell cycle analysis. On the basis of the present data, we propose that the biological effects of nanoparticles may be mediated through two distinct mechanisms, involving contributions from both the nanoparticle core and the physicochemical properties imparted by surface functionalization. Future research will focus on further reducing the toxicity of AgNPs toward normal cells while enhancing their selective anticancer efficacy.

2. Materials and Methods

2.1.Chemicals

Analytical-grade silver nitrate was obtained from the Shanghai Institute of Fine Chemical Materials and used as the silver precursor for the synthesis of AgNPs. Curcumin was purchased from Shanghai Yuanye Bio-Technology Co., Ltd. Sodium borohydride ($NaBH_4$) was acquired from Duksan Pure Chemicals (Republic of Korea) and employed to enhance the reduction efficiency of Ag^+. CCK reagent, RNase, fetal bovine serum (FBS), antibiotic-antimycotic solution, RPMI 1640, and DMEM medium were purchased from Mediatech, Inc.

2.2. AgNP Characterization

Transmission electron microscopy (TEM, TSM6360) was employed to characterize the size and dispersion of AgNPs. The optical properties of AgNPs were analyzed using a TU-1901 double-beam UV-Vis spectrophotometer (Beijing General Analysis Instrument Co., Ltd.). The silver content of the nanoparticles was determined by atomic absorption spectrometry (AAS). X-ray diffraction (XRD) patterns were collected on a Bruker D8 Advance diffractometer equipped with a Göbel mirror, using Cu Kα radiation.

2.3.AgNPs Synthesis

Briefly, a 5 mL ethanol solution containing 500 μg/mL $AgNO_3$ was mixed with 20 mL ethanol solutions containing 100, 200, 300, 400, 500, and 1000 μg/mL curcumin at room temperature under constant stirring. The mixture was reacted at 45 ℃for 2 h to prepare silver nanoparticle colloids. The AgNP suspension was centrifuged at 10,000 rpm for 30 min, and the supernatant was discarded to remove residual polymer and small-molecule reducing agents. The resulting precipitate was redispersed in 5 mL deionized water. The silver content of the nanoparticles was determined by atomic absorption spectrometry.

2.4. AgNPs Synthesis with $NaBH_4$

First, 1000 μg/mL curcumin was fully dissolved in 40 mL deionized water over 5 min. Subsequently, 5 mL aqueous silver nitrate ($AgNO_3$) solution (500 μg/mL) was added dropwise to the curcumin solution under magnetic stirring. After 30 min, 5 mL freshly prepared $NaBH_4$ solution was introduced into the mixture. The molar ratios of Ag^+ to $NaBH_4$ were set at 5:1, 4:1, 3:1, 2:1, 1:1, 1:2, and 1:3, respectively. The total volume of the reaction system was adjusted to 50 mL. The mixture was stirred at 45 ℃ for 2 h to ensure complete reduction.The resulting AgNP colloidal suspension was centrifuged at 10,000 rpm for 30 min, and the supernatant was discarded to remove residual curcumin and unreacted small-molecule reducing agent. The precipitate was then redispersed in 5 mL deionized water. The silver content of the nanoparticles was determined by atomic absorption spectrometry.Scheme 1 illustrates the synthetic procedure for curcumin-stabilized silver nanoparticles (cAgNPs).

2.5. Cell Culture

Human bronchial epithelial (HBE) cells and human lung squamous carcinoma (HTB-182) cells were provided by the Cell Bank of the Advanced Research Center, Central South University.HBE cells were cultured in Gibco Modified Eagle's Medium (MEM) supplemented with 4.5 g/L glucose, sodium pyruvate, 10% (v/v) fetal bovine serum (FBS), and 1% antibiotic-antimycotic solution (all from Mediatech). Cells were maintained at 37°Cin a humidified incubator with 5% CO_2.HTB-182 cells were cultured in RPMI-1640 complete medium under identical incubation conditions (37°C, 5% CO_2, humidified atmosphere). The medium was supplemented with 2.2% (w/v) sodium bicarbonate, 0.03% (w/v) L-glutamine, 100 units/mL penicillin, 100 µg/mL streptomycin, and 10% fetal bovine serum.

2.6. CCK-8 Test Assay

Cell viability following treatment with modified nanoparticles was evaluated using a Cell Counting Kit-8 (CCK-8) assay, with untreated cells serving as the control group. For each assay, cells were seeded into 96-well plates (Nalge Nunc) at a density of 5.0×10^3 cells/cm² and cultured for 24 h. The nanoparticle conjugates were mixed with DMEM at a ratio of 1:4 (v/v) prior to administration. Cells were then incubated at 37 ℃ in a 5% CO_2 humidified atmosphere for an additional 24 h. Subsequently, 10 µL of CCK-8 reagent was added to each well, and the plates were incubated for a further 4 h. Cell viability was calculated as the percentage ratio of the absorbance of treated cells relative to that of untreated control cells.
Inhibition rate= (ODc-ODt)/ODc×100%
where ODc and ODt are the OD 490 nm values of the control group without any treatment and the treatment group (either the curcumin-Ag group or the silver ion group), respectively.

2.7. Cell Death-Propidium Iodide (PI) Staining

Twenty-four hours after seeding in 6-well plates, cells were treated with 5 ppm AgNPs for a further 24 h. After treatment, cells were washed twice with cold PBS and resuspended in 1× binding buffer at a density of 1×10^6 cells/mL. An aliquot (100 µL) of the cell suspension was incubated with 5 µL propidium iodide (PI) at room temperature for 15 min in the dark. Afterwards, the cell suspension was diluted with 400 µL of 1× binding buffer. Fluorescence intensity was measured using an LSR II flow cytometer (Becton Dickinson). Data acquisition and analysis were performed using BD FACS Diva software (version 6.0, Becton Dickinson), with 10,000 events collected per sample.

2.8. Cell Cycle Analysis with Flow Cytometry

Cells were cultured in DMEM for 24 h and then treated with AgNPs in fresh DMEM for an additional 24 h. After incubation with AgNPs, cells were fixed in pre-chilled 70% ethanol at − 20 ℃ and stored until analysis.For cell cycle analysis, fixed cell suspensions were centrifuged at 1,250 rpm for 12 min, and the cell pellet was resuspended in PBS. Cells were then incubated with 200 µg/mL RNase (Sigma) at 37 ℃ for 30 min. After RNase digestion, cells were stained with 100 µg/mL propidium iodide (PI, Sigma) at room temperature for 15 min in the dark.Cell cycle distribution was analyzed using a BD LSR II flow cytometer (BD Biosciences) equipped with a 488 nm excitation laser and PE channel fluorescence detection. Data were processed and analyzed using FlowJo software (FlowJo, LLC).

2.9. Statistical Analysis

Statistical analyses were performed using SPSS software (version 16.0; SPSS Inc., Chicago, IL, USA). A one-way analysis of variance (ANOVA) was employed to assess statistical significance, which was defined as a p-value < 0.05.

3. Results and discussion

3.1. Physical and Chemical Properties of Curcumin modified Nano Silver

Figure 1A (left) shows TEM images of curcumin-stabilized AgNPs prepared without reducing agent, while Fig. 1A (right) displays those synthesized with reducing agent. The formation efficiency of AgNPs was relatively low in the absence of reducing agent, resulting in only a small number of nanoparticles observed in the TEM field, with an average diameter of 15 nm. In contrast, a large quantity of uniformly dispersed AgNPs with an average size of 30 nm was obtained when reducing agent was added(Fig. 1A, right). Figure 1B(left) presents the UV-Vis absorption spectra of curcumin-AgNPs prepared at low curcumin concentrations (100–500 ppm) without reducing agent. At these low concentrations, curcumin acted as both a reducing agent

and a capping agent, leading to the formation of curcumin-coated AgNPs. These results confirm that curcumin can reduce Ag^+ions from silver nitrate to elemental silver nanoparticles, owing to the presence of reductive functional groups such as ketone moieties.

Next, the curcumin concentration was increased to 1000 ppm. The resulting data revealed that a higher curcumin concentration favored the formation of AgNPs. However, the yield of silver nanoparticles no longer increased once the curcumin concentration reached 1000 ppm. Accordingly, 1000 ppm was chosen as the optimal curcumin concentration for subsequent experiments.Nanosilver was also prepared by varying the mass ratio of silver to sodium borohydride. Figure 1B (right) shows the UV-Vis absorption spectra of curcumin-capped AgNPs synthesized with different Ag:$NaBH_4$ ratios (5:1, 4:1, 3:1, 2:1, 1:1, 1:2, and 1:3). The black curve represents AgNPs prepared in the absence of reducing agent. In the absence of $NaBH_4$, nanoparticle formation efficiency was relatively low, the absorption peak was broad, and the maximum absorbance was below 0.5. Upon addition of $NaBH_4$, the characteristic surface plasmon resonance peak of AgNPs gradually intensified. The strongest absorption peak was observed at an Ag:$NaBH_4$ ratio of 1:1. With further increases in $NaBH_4$(ratios 1:2 and 1:3), excessive reduction induced silver precipitation, resulting in lower characteristic absorption peaks compared with the 1:1 ratio.XRD patterns of the AgNPs exhibited two obvious Bragg reflections, which were indexed to the face-centered cubic(fcc) crystal structure of silver. The diffraction peaks at 38.13°and 43.92°were assigned to the (111) and (200) planes, respectively, confirming the crystalline nature of the biosynthesized AgNPs (Fig. 2A). These results indicate that the nanoparticles possessed good crystallinity with a cubic structure, and the diffraction angles were consistent with those of bulk silver. Figure 2B shows the ^1H NMR spectra of pure curcumin and curcumin-AgNPs. The oxygen atoms in the ketone groups of curcumin coordinated with silver, enabling curcumin to cap the surface of AgNPs. Hydroxyl and methoxy groups in the curcumin molecules were largely preserved.

3.2. Cytotoxic Effects of Nano-Ag on Normal HBE Cells

3.2.1. Cell Morphology and CCK Test

The first and most immediately noticeable effect of exposing cells to toxic substances is an alteration in cell shape or morphology in monolayer culture. Figure 3 presents representative micrographs of HBE cells treated with different concentrations of curcumin-modified silver nanoparticles (curcumin-AgNPs) and curcumin for 24 h. Curcumin samples were diluted to concentrations of 312.5, 625, 937.5, 1250, 1562.5, 1875, and 2500 ppm, followed by co-culture with normal HBE cells for 24 h.As shown in the micrographs, HBE cells in the control group exhibited an irregular polygonal shape with uniform size, clear contours, and adherent growth. HBE cells maintained good growth status at a curcumin concentration of 1875 ppm. In contrast, when the curcumin concentration reached 2500 ppm, only a small number of cells showed morphological changes, including cell shrinkage and nuclear condensation.

Microscopic observation of treated cells revealed distinct morphological alterations indicative of cellular injury, whereas control cells retained a normal phenotype. Cells exposed to AgNPs exhibited extensive clustering, reduced cellular protrusions, and limited cell spreading relative to untreated control cells. These changes may be attributed to disruption of cytoskeletal function induced by nanoparticle treatment.The cell density was markedly reduced following AgNP exposure, and some dark crystalline aggregates were visible on the cell surface. In all AgNP-treated groups shown in Fig. 3, cells exhibited severe morphological disruption and complete loss of cytoplasmic integrity. The dark patches observed on the cell surface likely reflect adsorption and accumulation of nanoparticles. Nevertheless, only a small number of floating cells were detected microscopically, indicating that extensive necrotic cell death was absent and that cell death occurred mainly via apoptosis.

Although optical microscopy can directly reflect the cytotoxic effects of nanosilver toward cells, the CCK-8 assay provides a more quantitative and reliable method to evaluate cell viability and inhibitory effects. Accordingly, CCK-8 assays were performed to assess the cytotoxicity of curcumin-modified AgNPs and silver ions in HBE cells. Cells were exposed to serial concentrations of 2, 4, 8, 10, 15, 20, 30, 40, and 50 ug/mL for 24 h. The inhibitory rates of curcumin-AgNPs and curcumin toward HBE cells are summarized in Table 2 and visualized in Figs. 5A and 5B.The half-maximal inhibitory concentration (IC_{50}) values were determined to be 13.65 ug/mL for curcumin-modified AgNPs and 5.39 ug/mL for silver ions, respectively. The inhibitory rate increased in a dose-dependent manner with increasing concentrations of both AgNPs and silver ions. Notably, cytotoxicity

differed markedly between treatments with curcumin-AgNPs and silver ions, particularly in the AgNP-treated groups. The inhibitory rate against HBE cells exceeded 80% at AgNP concentrations above 30 ug/mL, whereas the same level of inhibition was achieved at only 10 ug/mL for silver ions.An inhibitory rate greater than 80% is generally regarded as significant cytotoxicity at a given nanoparticle concentration[36]. These findings are consistent with the morphological changes observed in AgNP-treated cells(Fig. 3). To our knowledge, nanoparticle uptake becomes saturated at higher concentrations, and excess nanoparticles tend to aggregate and bind to specific sites on the cell membrane. Our results are in good agreement with previous reports highlighting the critical role of surface chemistry in cellular internalization: highly positively charged particles show the highest uptake efficiency, whereas particles with a near-zero zeta potential exhibit lower cellular uptake.

Table 2
Inhibition rate of curcumin silver and curcuminon HBE after 24-hour

Inhibition rate of curcumin modified silver nanoparticles on normal HBE cells											
Concentration(ug/mL)	**50**	**40**	**30**	**20**	**15**	**10**	**8**	**4**	**2**	**0**	**IC_{50}**
Absorbance	**0.204**	**0.217**	**0.254**	**0.626**	**0.826**	**1.01**	**1.339**	**1.392**	**1.424**	**1.524**	
24h inhibition rate(%)	**86.56**	**85.7**	**83.28**	**58.87**	**45.8**	**33.68**	**12.08**	**8.86**	**6.56**	**0**	**16**
Inhibition rate of silver ion on normal HBE cells											
Concentration(ug/mL)	**50**	**40**	**30**	**20**	**15**	**10**	**8**	**4**	**2**	**0**	**IC_{50}**
Absorbance	**0.165**	**0.171**	**0.172**	**0.179**	**0.181**	**0.189**	**0.391**	**1.040**	**1.286**	**1.381**	
24h inhibition rate(%)	**88.54**	**88.13**	**88.06**	**87.57**	**87.43**	**86.88**	**72.86**	**27.80**	**10.75**	**0**	**5.39**
Inhibition rate of curcumin on HBE cells											
Concentration(ug/mL	**100**	**80**	**60**	**40**	**30**	**20**	**15**	**10**	**5**	**0**	**IC_{50}**
Absorbance	**0.507**	**0.673**	**0.818**	**1.007**	**1.141**	**1.311**	**1.381**	**1.404**	**1.437**	**1.524**	
24h inhibition rate(%)	**66.7**	**55.8**	**46.3**	**33.9**	**25.09**	**13.96**	**9.38**	**7.82**	**5.65**	**0**	**69.7**

3.2.2. Apoptosis and Necrosis

Flow cytometric analysis of FITC-Annexin V/PI-stained HBE cells is presented in Figs. 6D, 6E, and 6F. In contrast to cancer cells, no significant difference was observed in the early apoptosis rate of HBE cells treated with curcumin-modified AgNPs versus silver ions (53.3% vs. 47.9%, respectively). However, the effect of silver ions on late apoptosis and necrosis was significantly higher than that of curcumin-modified AgNPs (19.1% vs. 5.18%, respectively; $p < 0.05$).Notably, silver ions exhibited greater cytotoxicity when considering the total apoptosis and necrosis rate: curcumin-modified AgNPs induced a total apoptosis and necrosis rate of 58.4%, whereas silver ions induced a rate of 67%. These results indicate that silver ions are more toxic to normal human bronchial epithelial (HBE) cells than curcumin-modified AgNPs, which is consistent with the findings from the CCK-8 assay.

3.2.3. Effect on Cell Cycle

To investigate the potential DNA damage induced by oxidative stress in Ag nanoparticle (AgNP)-treated HBE cells, cell cycle distribution was monitored via flow cytometry by measuring DNA content. Cell proliferation primarily consists of four phases: G1 phase (cellular growth), S phase (DNA synthesis), G2 phase (preparatory stage for cell division), and M phase (mitosis).Flow cytometric analysis results are presented in Figs. 7A, 7B, and 7C. As shown in Fig. 7G, the cell cycle distribution of HBE cells was most notably affected when exposed to AgNPs at a concentration of 5 ppm.Compared with untreated control cells, different surface-modified AgNPs exerted distinct effects on the cell cycle of HBE cells.After AgNP exposure, a significant increase in the proportion of HBE cells in the sub-G1 phase was observed, and the apoptosis-related data further indicated that bronchial epithelial cells were arrested in the G0/G1 phase. Specifically, following AgNP intervention, the proportion of HBE cells in the

G0/G1 phase increased from the baseline 24.81% to 49.25% in the curcumin-modified AgNP group and to 54.95% in the Ag^+ group, respectively.

3.3. Cytotoxic Effects of Nano-Ag on Lung Squamous Cell Carcinoma

3.3.1. Cell Morphology and CCK test

Lung cancer is clinically classified into non-small cell lung cancer (NSCLC) and small cell lung cancer (SCLC). NSCLC accounts for approximately 80% of all lung cancer cases, with around 75% of patients diagnosed at an advanced stage, resulting in a very low 5-year survival rate. NSCLC can be further subdivided into squamous cell carcinoma (SCC), adenocarcinoma, and large cell carcinoma. Compared with SCLC, NSCLC cells exhibit slower proliferation and relatively late metastasis.Among NSCLC subtypes, lung squamous cell carcinoma (LSCC) is associated with a lower survival rate than adenocarcinoma and has an extremely low EGFR mutation rate, which provides no significant predictive value for targeted therapy. Furthermore, compared with non-squamous cell carcinoma, research on LSCC remains relatively limited, and there is a lack of effective molecular targeted drugs for its treatment. Therefore, HTB-182 cells were selected in this study to investigate the anticancer effect of silver nanoparticles (AgNPs) on lung squamous cell carcinoma.

The first and most immediately noticeable effect following exposure of cells to toxic materials was an alteration in cell shape or morphology in monolayer culture. Figure 4 presents representative micrographs of HTB-182 cells treated with different concentrations of curcumin-modified silver nanoparticles for 24 hours. Microscopic observation revealed distinct morphological changes in the treated cells, whereas the control cells maintained a normal appearance.Cells treated with silver nanoparticles (AgNPs) showed clustered growth with reduced cellular extensions, and their ability to spread was restricted, which might be attributed to disrupted cytoskeletal function induced by AgNP treatment. A significant decrease in the number of viable cells was observed in the AgNP-treated groups, and black crystal-like aggregates were visible on the cell surface.In all AgNP-treated groups, cells exhibited obvious morphological damage, including complete collapse of cell structure and loss of cytoplasmic integrity. The dark patches observed on the cell surface were likely due to the adsorption and accumulation of AgNPs. Notably, only a small number of floating cells were detected, indicating that widespread apoptotic cell death did not occur.

Although optical microscopy images can directly reflect the cytotoxicity of nanosilver to cells, the CCK-8 assay provides a more convenient and quantitative method to assess cell inhibitory effects. We performed CCK-8 assays to determine the cytotoxicity of curcumin-modified silver nanoparticles (curcumin-AgNPs) and silver ions in HTB-182 cells. Curcumin-AgNPs and silver ions were serially diluted to concentrations of 2, 4, 8, 10, 15, 20, 30, 40, and 50 μg/mL, and the results are presented in Fig. 4. The inhibitory rates of curcumin-AgNPs and curcumin on HTB-182 cells after 24 h of treatment are summarized in Table 3.The inhibitory rate increased in a dose-dependent manner with increasing concentrations of both curcumin-AgNPs and silver ions. Notably, there were significant differences in cytotoxicity between curcumin-AgNP and silver ion treatments. The inhibitory rate against HTB-182 cells exceeded 80% when the curcumin-AgNP concentration was above 25 μg/mL and when the silver ion concentration was 20 μg/mL. An inhibitory rate greater than 80% is generally regarded as significant cytotoxicity at a given nanoparticle concentration. These findings are consistent with the morphological changes observed in AgNP-treated HTB-182 cells (Fig. 4). Specifically, as shown in Fig. 4B4 (25 μg/mL), curcumin-AgNPs exhibited significant cytotoxic effects on HTB-182 cells at concentrations above 25 μg/mL, whereas silver ions exerted significant cytotoxicity at concentrations above 20 μg/mL.To our knowledge, nanoparticle uptake by cells becomes saturated at higher concentrations, and excess nanoparticles tend to assemble in a characteristic pattern and anchor to specific sites on the cell membrane. Our results are in good agreement with previous reports highlighting the decisive role of nanoparticle surface chemistry in cellular uptake: highly positively charged particles exhibit the highest uptake efficiency, while particles with a zeta potential close to zero are less readily taken up by cells. It is conceivable that curcumin-AgNPs were better retained or attached to cells through electrostatic interactions between the negatively charged cell membrane and the cationic coating of the nanoparticles. Compared with other biological polymers, curcumin-AgNPs showed higher affinity for proteins present in the cellular medium, which prolongs their retention and contributes to enhanced cellular uptake.

Table 3
Inhibition rate of curcumin silver and curcumin on HTB-182 after 24-hour

Inhibition rate of curcumin modified silver nanoparticles on HTB182 cells											
Concentration(ppm)	**50**	**40**	**30**	**20**	**15**	**10**	**8**	**4**	**2**	**0**	**IC_{50}**
Absorbance	**0.114**	**0.130**	**0.408**	**0.449**	**0.556**	**0.654**	**0.676**	**0.799**	**0.820**	**0.979**	
24h inhibition rate(%)	**88.3**	**86.7**	**58.3**	**54.1**	**43.2**	**33.18**	**30.9**	**18.3**	**16.2**	**0**	**17.6ppm**
Inhibition rate of silver ion on HTB182 cells											
Concentration(ppm)	**50**	**40**	**30**	**20**	**15**	**10**	**8**	**4**	**2**	**0**	**IC_{50}**
Absorbance	**0.119**	**0.120**	**0.120**	**0.122**	**0.427**	**0.618**	**0.649**	**0.833**	**0.902**	**0.979**	
24h inhibition rate(%)	**87.78**	**87.68**	**87.66**	**87.43**	**56.2**	**36.66**	**33.45**	**14.63**	**7.54**	**0**	**11.3ppm**
Inhibition rate of curcumin on HTB182 cells											
Concentration(ppm)	**50**	**40**	**30**	**20**	**15**	**10**	**8**	**4**	**2**	**0**	**IC_{50}**
Absorbance	**0.334**	**0.494**	**0.521**	**0.628**	**0.721**	**0.842**	**0.928**	**0.940**	**0.965**	**0.979**	
24h inhibition rate(%)	**65.8**	**49.5**	**46.7**	**35.8**	**26.3**	**13.9**	**5.09**	**3.96**	**1.38**	**0**	**42.6ppm**

In Fig. 5, concentration-response curves were plotted using SPSS software to calculate the half-maximal inhibitory concentration (IC_{50}) values. The results showed that the IC_{50} of curcumin-modified silver nanoparticles against HTB-182 cells was 17.6 ug/mL, while the IC_{50} of silver ions was 11.3 ug/mL. These data strongly indicate that the silver nanoparticles(AgNPs) possess anticancer potential. This finding demonstrates that surface modification of silver nanoparticles significantly influences their tumor-suppressive, anticancer, and antiproliferative properties.We further compared the IC_{50} values of silver nanoparticles with those of a clinically mature anti-lung cancer drug, dichlorodiammineplatinum(DDP, cisplatin). The average inhibitory concentration of silver nanoparticles was 10 times lower than that of cisplatin. These results suggest that silver nanoparticles have the potential to be developed as a novel anti-lung cancer agent.

3.3.2. Apoptosis and Necrosis

The apoptotic cell death of HTB-182 cells induced by silver nanoparticles (AgNPs) was confirmed via flow cytometric analysis using annexin V-FITC/PI staining. To evaluate the extent and mode of cell death, annexin V-FITC/PI staining was performed. Statistical data were extracted from the dot plots (Fig. 6) using FlowJo software. Flow cytometric analysis results of annexin V-FITC/PI-stained HTB-182 cells are presented in Figs. 6A, 6B, and 6C.The data from the annexin V-FITC/PI staining experiment indicated that only a small percentage of HTB-182 cells underwent necrosis when treated with all AgNP formulations and Ag^{+} at a concentration of 5 ug/mL. However, the degree of apoptosis varied among HTB-182 cells treated with different nanosilver formulations. For HTB-182 lung cancer cells, the survival rate was 31.9%. Notably, curcumin-modified AgNPs (curcumin-AgNPs) exhibited higher cytotoxicity, as the number of late apoptotic and necrotic cells was significantly higher than that in the silver ion group (curcumin-AgNPs vs. silver ions: 67.5% vs. 57.1%, $p < 0.05$). Specifically, the total apoptosis and necrosis rate was 68.2% in the curcumin-AgNP group and 62.14% in the silver ion group.These results demonstrate that AgNPs can induce cellular apoptosis, and the apoptotic response of HTB-182 cells varies with different silver formulations. This finding is consistent with the results of the CCK-8 assay.

3.3.3. Effect on Cell Cycle

To investigate potential DNA damage induced by oxidative stress in HTB-182 cells treated with silver nanoparticles (AgNPs), cell cycle distribution was monitored by measuring DNA content using a flow cytometer. Figures 7D, 7E, and 7F illustrate the effect of AgNPs on the cell cycle distribution of HTB-182 cells, based on flow cytometry data. Flow cytometric analysis (Fig. 7H) revealed

that the distribution of cells across different cell cycle phases (G0/G1, S, and G2/M) was most significantly affected when HTB-182 cells were exposed to AgNPs at a concentration of 5 ppm.Compared with untreated control cells, different surface-modified silver nanoparticles exerted distinct effects on cell cycle distribution. Specifically, HTB-182 cells (a non-small cell lung cancer cell line) were arrested in the G2/M phase following AgNP treatment. After intervention with AgNPs, the proportion of HTB-182 cells in the G2/M phase increased from 13.52% to 16.2% in the curcumin-modified AgNP group and to 16.5% in the Ag^+ group, respectively. These results are consistent with previous findings reported in the literature [35].Notably, the cytotoxicity of AgNPs to HTB-182 cells was positively correlated with the proportion of cells arrested in the cell cycle: the more potent the cytotoxicity of the AgNPs, the higher the proportion of cells undergoing cell cycle arrest. In fact, current cancer therapeutic strategies heavily rely on DNA-damaging agents to induce programmed cell death (apoptosis) in cancer cells.

4. Conclusions

It is well recognized that the biokinetics of nanoparticles—defined as the rate of nanoparticle uptake, intracellular distribution, and exocytosis—plays a crucial role in their toxic effects. Key factors influencing nanoparticle biokinetics and toxicity include particle size, surface area, and surface functionalization. Notably, the inhibitory rate of cells increased in a concentration-dependent manner with increasing concentrations of nanosilver and silver ions.CCK-8 assay results showed that the half-maximal inhibitory concentration(IC_{50}) of curcumin-modified silver nanoparticles (curcumin-AgNPs) on normal human bronchial epithelial (HBE) cells was 13.65 ug/mL, while the IC_{50} of silver ions on HBE cells was 5.39 ug/mL. For lung squamous cell carcinoma cells (HTB-182), the IC_{50} of curcumin-AgNPs was 17.6 ug/mL, and the IC_{50} of silver ions was 11.3 ug/mL. These findings suggest that nanosilver could serve as a novel option for the treatment of lung squamous cell carcinoma, highlighting the practical significance of applying nanosilver in the clinical management of this disease to mitigate toxic side effects.Our results further demonstrate that surface modification of silver nanoparticles significantly affects their anticancer and antiproliferative activities. Specifically, treatment with nanosilver or silver ions induced cell cycle arrest in HBE cells at the G0/G1 phase, whereas in non-small cell lung cancer HTB-182 cells, the cell cycle arrest occurred at the G2/M phase, which is associated with DNA damage repair processes. These observations indicate that the mechanism of action of silver ions and silver nanoparticles differs between normal HBE cells and lung cancer cells.Previous studies have reported the detection of apoptosis-related proteins[37–39]. Therefore, future research should focus on elucidating the detailed anticancer mechanism of nanosilver and further reducing the toxicity of silver nanoparticles to normal cells.

Declarations

Notes

The authors declare no competing financial interest.

Ethics declaration: not applicable.

Consent for Publication:All authors have given their consent for publication.

Consent for Publication:

All authors have given their consent for publication.

Author Contribution

Wei Su:Experimental methods and paper writing；Bai Lin Dai：data analysis；Li Tang：data analysis；Li Bo Nie：article review；Jian Xin Tang：funding support

Acknowledgements:

This work was supported by Natural Science Foundation of Hunan Province (2024JJ7133),Excellent Youth Program of Hunan Provincial Department of Education(23B0561), Natural Science Foundation of Hunan Province(2022JJ50099, 2024JJ7137), Key Research and Development Program of Hunan Province (2022SK2009),Shenzhen Longgang District Special Fund for Technological Innovation: Medical and Health Technology Research Project(LGKCYLWS2023031).

References

1. Jun YO, Han SK, Palanikumar L, Eun MG, Batakrishna J, Soo AP, Ho YK, Kibeom K, Jeong KS, Sang KK, Chaekyu K, Sebyung K, Ja-Hyoung R(2018)Cloaking nanoparticles with protein corona shield for targeted drug delivery. Nat Commun, 9:4548–4557https://doi.org/10.1038/s41467-018-06979-4
2. Wei M, Li S, Le WD(2017)Nanomaterials modulate stem cell differentiation: biological interaction and underlying mechanisms. J Nanobiotechnol 15:75–88https://doi.org/10.1186/s12951-017-0310-5
3. Song JY, Zhu YN, Zhang JM, Yang J, Du Y, Zheng WW, Wen CY, Zhang YM, Zhang L (2019) Encapsulation of AgNPs within Zwitterionic Hydrogels for Highly Efficient and Antifouling Catalysis in Biological Environments.Langmuir. 5:1563–1570. https://doi.org/10.1021/acs.langmuir.8b02918
4. Liu ZX, Tia S, Li Q, Wang JC, Pu JB, Wang G, Zhao WJ, Feng F, Qin J Ren LC(2020)Integrated Dual-Functional ORMOSIL Coatings with AgNPs@rGO Nanocomposite for Corrosion Resistance and Antifouling Applications. ACS Sustain Chem Eng 8: 6786–6797https://doi.org/10.1021/acssuschemeng. 0c01294
5. Núñez-Martínez M, Arias S, Quiñoá E, Riguera R, Freire F (2021))Dynamic Chiral PPA–AgNP Nanocomposites: Aligned Silver Nanoparticles Decorating Helical Polymers. Chem Mater 33:4805–4812. https://doi.org/10.1021/acs.chemmater. 1c00805
6. Karade VC, Patil RB, Parit SB, Jin HK, Chougale AD, Dawkar VV (2021) Insights into Shape-Based Silver Nanoparticles: A Weapon to Cope with Pathogenic Attacks. ACS Sustain Chem Eng 9:12476–12507. https://doi.org/10.1021/acssuschemeng.1c03797
7. Zhang YP, Pan XH, Liao SJ, Jiang CY, Wang LQ, Tang YR, Wu GJ, Dai G, Chen LY(2020)Quantitative Proteomics Reveals the Mechanism of Silver Nanoparticles against Multidrug-Resistant Pseudomonas aeruginosa Biofilms. J Proteome Res, 19:3109–3122https://doi.Org/10.1021/acs. jproteome. 0c00114
8. Nycz M, Arkusz K, Pijanowska DG (2021) Electrodes Based on a Titanium Dioxide Nanotube–Spherical Silver Nanoparticle Composite for Sensing of Proteins. ACS Biomater Sci Eng 7:105–113. https://doi.org/10.1021/acsbiomaterials.0c01207
9. Zhou WH, Jia ZJ, Xiong P, Yan JL, Li YY, Li M, Cheng Y, Zheng YF(2017)Bioinspired and Biomimetic AgNPs/Gentamicin-Embedded Silk Fibroin Coatings for Robust Antibacterial and Osteogenetic Applications. ACS Appl Mater Interfaces, 9:25830–25846https://doi.Org/10.1021/acsami.7b06757
10. Sarkar AK, Saha A, Midya L, Banerjee C, Mandre N, Panda AB, Pal S(2017)Cross-Linked Biopolymer Stabilized Exfoliated Titanate Nanosheet-Supported AgNPs: A Green Sustainable Ternary Nanocomposite Hydrogel for Catalytic and Antimicrobial Activity. ACS Sustain Chem Eng, 5:1881–1891. https://doi.org/10.1021/acssuschemeng.6b02594
11. Wu ZG, Zhou W, Deng WJ, Xu CL, Cai Y, Wang XY(2020)Antibacterial and Hemostatic Thiol-Modified Chitosan-Immobilized AgNPs Composite Sponges. ACS Appl Mater Interfaces, 12:20307–20320https://doi.Org/10.1021/acsami.0c05430
12. Khamrai M, Banerjee SL, Paul S, Ghosh AK, Sarkar P, Kundu PP (2021)AgNPs Ornamented Modified Bacterial Cellulose Based Self-Healable L-B-L Assembly via a Schiff Base Reaction: A Potential Wound Healing Patch.ACS Appl Bio Mater, 4:428–440. https://doi.Org/10.1021/acsabm. 0c00915
13. Wang FY, Yan BB, Li ZR, Wang P, Zhou M, Yu YY, Yuan JG, Cui L, Wang Q (2021)Rapid Antibacterial Effects of Silk Fabric Constructed through Enzymatic Grafting of Modified PEI and AgNP Deposition. ACS Appl Mater Interfaces, 13:33505–33515. https://doi.org/10.1021/acsami. 1c08119
14. Peng L, Luo Y, Zheng YQ, Zhang WD, Chen GJSunlight-Induced RAFT Synthesis of Multifaceted Glycopolymers with Surface Anchoring, In Situ AgNP Formation, and, Properties A (2018) ACS Appl Nano Mater, 1: 2219–2226.https://doi.org/10.1021/acsanm.8b00286
15. Foldbjerg R, Dang DA, Autrup H(2011)Cytotoxicity and genotoxicity of silver nanoparticles in the human lung cancer cell line. A549 Arch Toxicol, 85(7)743–750https://doi.org/10.1007/s00204-010-0545-5

16. Valodkar M, Jadeja RN, Thounaojam MC, Devkar RV, Thakore S (2011) In vitro toxicity study of plant latex capped silver nanoparticles in human lung carcinoma cells. Mater Sci Eng C,31(8):1723–1728. https://doi.Org/10.1016/j.msec. 2011. 08.001
17. Pan XF, Yin HY (2014) Effect of silver nanoparticles on proliferation of human lung cancer A549 cells. J Pract Oncol 29(2):148–152
18. Meczynska-Wielgosz S, Wojewodzka M, Kruszewski M (2012) The effect of agglomeration state of silver and titanium dioxide nanoparticles on cellular response of HepG2, A549 and THP-1 cells.Toxicol Lett. 208(3):197–213. https://doi.org/10.1016/j.toxlet.2011.11.006
19. Gengan RM, Anand K, Phulukdaree A, Chuturgoon A (2013) A549 lung cell line activity of biosynthesized silver nanoparticles using Albizia adianthifolia leaf. Colloid Surf B 105(1):87–91
20. Boca SC, Potara M, Gabudean AM, Juhem A, Baldeck PL, Astilean S (2011) Chitosan-coated triangular silver nanoparticles as a novel class of biocompatible, highly effective photothermal transducers for in vitro cancer cell therapy. Cancer Lett 311(2):131–140
21. Ebrahimzadeh MA, Tafazoli A, Akhtari J, Biparva P, Eslami S(2018)Engineered silver nanoparticles a new nanoweapon against cancer. Anti-Cancer Agent Me, 18(14):1962–1969
22. Sankar R, Karthik A, Prabu A, Karthik S, Shivashangari KS, Ravikumar V(2013)Origanum vulgare mediated biosynthesis of silver nanoparticles for its antibacterial and anticancer activity. Colloid Surf B, 108(1): 80–84. https://doi.org/10.1016/j.colsurfb.2013.02.033
23. Venkatesan B, Subramanian V, Tumala A, Vellaichamy E (2014) Rapid synthesis of biocompatible silver nanoparticles using aqueous extract of Rosa damascena petals and evaluation of their anticancer activity. Asian Pac J Trop Med 7(1):294–300. https://doi.org/10.1016/s1995-7645
24. Chairuangkitti P, Lawanprasert ST, Roytrakul S, Aueviriyavit S, Phummiratch D, Kulthong K, Maniratanachote R (2013) Silver nanoparticles induce toxicity in A549 cells via ROS-dependent and ROS-independent pathways. Toxicol Vitro 27(1):330–338. https://doi.org/10.1016/j.tiv.2012.08.021
25. Oussef HF, Hegazy W, Abo-almaged HH(2015)Preparation and characterization of micronized zeolite Na-A: cytotoxic activity of silver exchanged form. J Porous Mat, 22(4):1033–1041https://doi.org/10.1007/s10934-015-9977 -x
26. Wang C, Tang F, Wang X, Li L (2015) Self-assembly of fluorescent hybrid core–shell nanoparticles and their application. ACS Appl Mater Interfaces 7(24):13653–13658. https://doi.org/10.1021/acsami.5b03440
27. Lankoff AL, Sandberg WJ, Wegierek-Ciuk A, Lisowska H, Refsnes B, Meczynska-Wielgosz S, Wojewodzka M, Kruszewski M (2012) The effect of agglomeration state of silver and titanium dioxide nanoparticles on cellular response of HepG2, A549 and THP-1 cells.Toxicol Lett. 208(3):197–213. https://doi.org/10.1016/j.toxlet.2011.11.006
28. Palaniappan P, Sathishkumar G, Sankar R (2015) Fabrication of nano-silver particles using Cymodocea serrulate and its cytotoxicity effect against human lung cancer A549 cells line. Spectrochimica Acta Part A 138(5):885–890. https://doi.org/10.1016/j.saa.2014.10.072
29. Matai I, Sachdev A, Gopinath P (2015) Multicomponent 5-fluorouracil loaded PAMAM stabilized-silver nanocomposites synergistically induce apoptosis in human cancer cells. Biomater Sci-Uk 3(3):457–468. https://doi.org/10.1039/C4BM00360H
30. Mehta HJ, Patel V, Sadikot RT(2014)Curcumin and lung cancer–a review. Target Oncol, 9:295–310https://doi.Org/10. 100/s11523-014-0321-1
31. Khoury EE, Abiad M, Kassaify ZG, Patra D (2015) Green synthesis of curcumin conjugated nanosilver for the applications in nucleic acid sensing and anti-bacterial activity. Colloid Surf B: Biointerfaces 127:274–280. https://doi.org/10.1016/j.colsurfb.2015.01.050
32. Ye MX, Li Y, Yin H, Zhang J (2012)Curcumin: Updated Molecular Mechanisms and Intervention Targets in Human Lung Cancer. Int J Mol Sci, 13,3959–3978https://doi.org/10.3390/ijms13033959
33. Cai Y, Wang J (2015) A preliminary study on radiosensitization effect of curcumin plus cisplatin on non-small cell lung cancer A549 cells. Chin Clin Oncol 20:13–17

34. Wang L, Zhang J, Cai L, Wen J, Shi H (2012) Liposomal curcumin inhibits Lewis lung cancer growth primarily through inhibition of angiogenesis. Oncol Lett 4:107–112
35. Liu ZG, Sun YS, Ren LQ, Huang Y, Cai YP, Weng QY, Shen XQ, Li XK, Liang G, Wang Y (2013) Evaluation of a curcumin analog as an anti-cancer agent inducing ER stress-mediated apoptosis in non-small cell lung cancer cells. BMC Cancer 13494. https://doi.org/10.1186/1471-2407-13-494
36. Vergne F, Quéré G, Andrieu-Key S, Descourt R, Quintin-Roué I, Talagas M, Braekeleer MD, Marcorelles P, Uguen A (2016) ALK-rearranged squamous cell lung carcinoma responding tocrizotinib: a missing link in the field of non-small cell lung cancer. Lung Cancer 91:67–69. https://doi.org/10.1016/j.lungcan. 2015.11.010
37. Ma J, Zhao D, Lu H, Huang W, Yu DH (2017) Apoptosis signal-regulating kinase 1 (ASK1) activation is involved in silver nanoparticles induced apoptosis of A549 lung cancer cell line. J Biomed Nanotechnol 13:349–354. https://doi.org/info:doi/10.1166/jbn.2017.2359
38. Wei X, Shao B, He, Ye T, Luo M (2015) Cationic nanocarriers induce cell necrosis through impairment of Na+/K+-ATPase and cause subsequent inflammatory response. Cell Res 25:237–253. https://doi.org/10.3410/f. 725325048.793528587
39. He W, Kienzle A, Liu X, Müller WE, Elkhooly TA, Feng QL (2016) In Vitro effect of 30 nm silver nanoparticles on adipogenic differentiation of human mesenchymal stem cells. J Biomed Nanotechnol 12:525–535. https://doi.org/10.1166/jbn.2016.2182

Scheme 1

Scheme 1 is available in the Supplementary Files section.

Figures

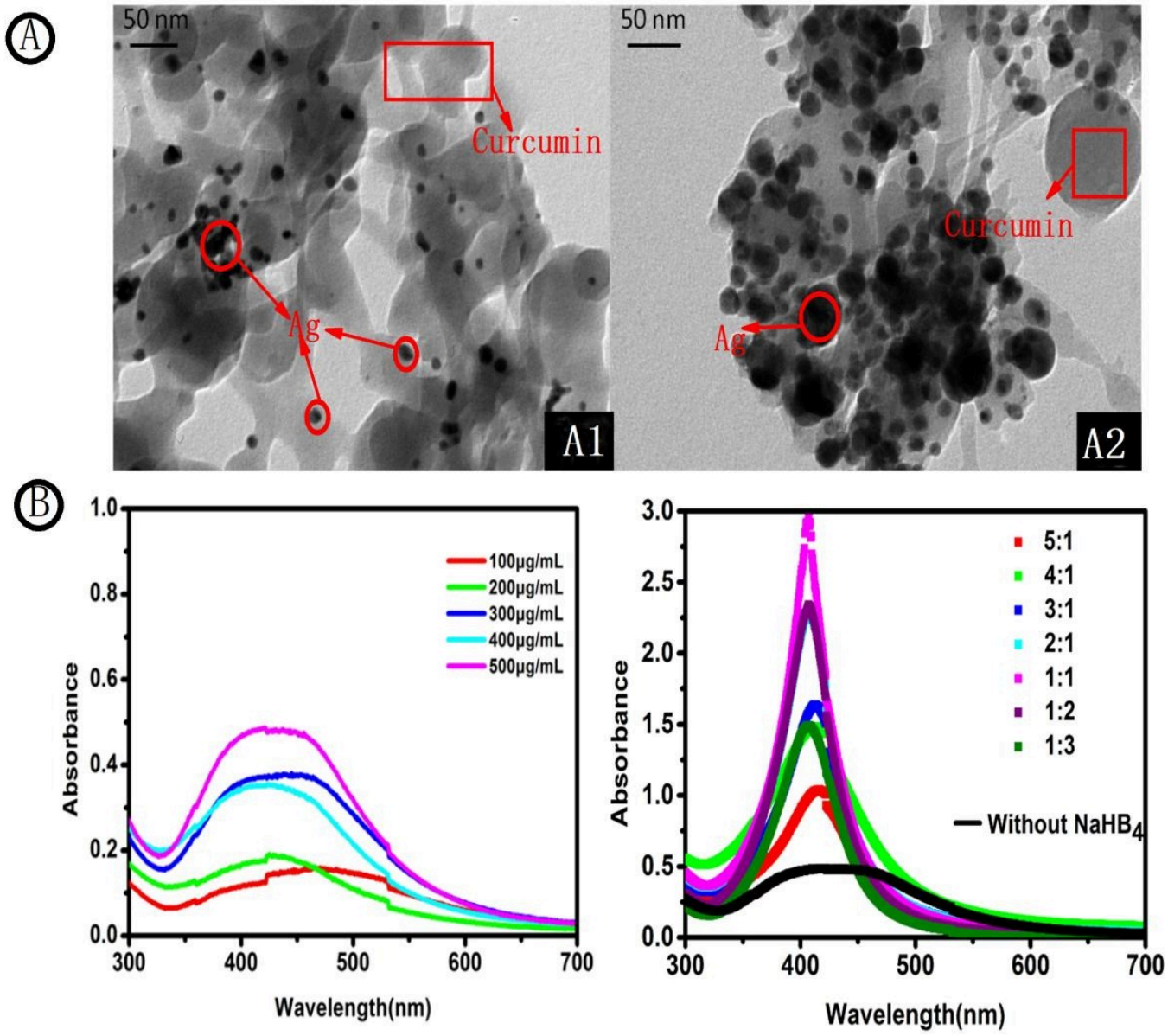


Figure 1

TEM images and UV-vis spectra of Curcumin-AgNPs. (A) TEM images of Curcumin-AgNPs after reaction for 2 hours at 45 °C. The concentration of Ag is 500 μg/mL. (B) UV-vis spectra of Curcumin-Ag reduced without a reducing agent and reduced with $NaBH_4$ after reaction for 2 hours at 45 °C. The concentration of Ag is 500 μg/mL and the dispersing solvent is water.

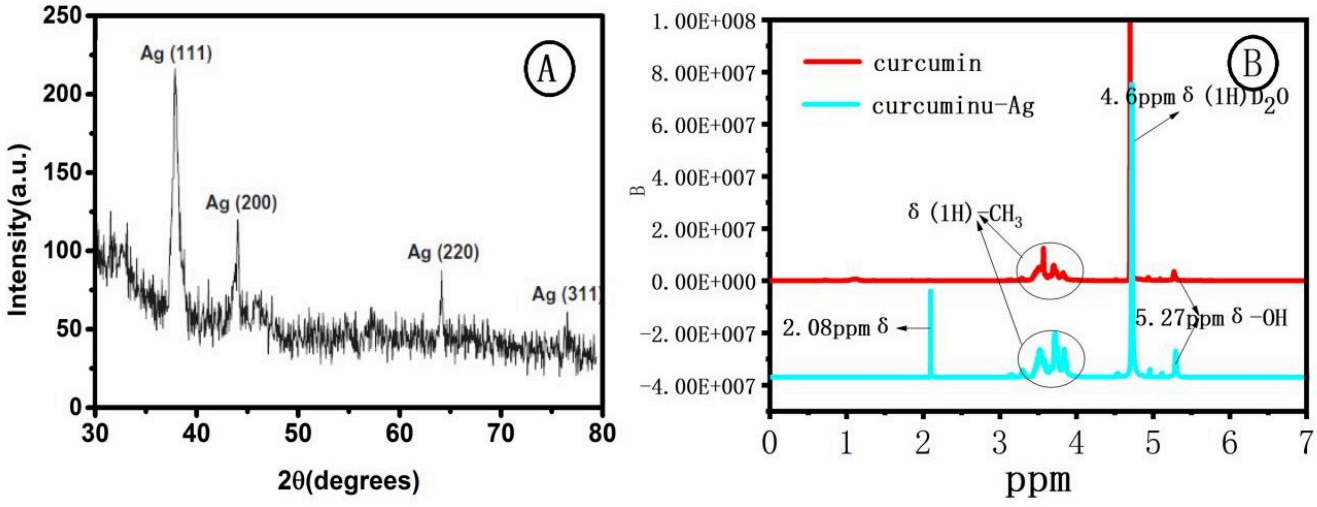


Figure 2

XRD pattern of the silver nanoparticles(A).1H NMR of curcumin and curcuminu-Ag(B)

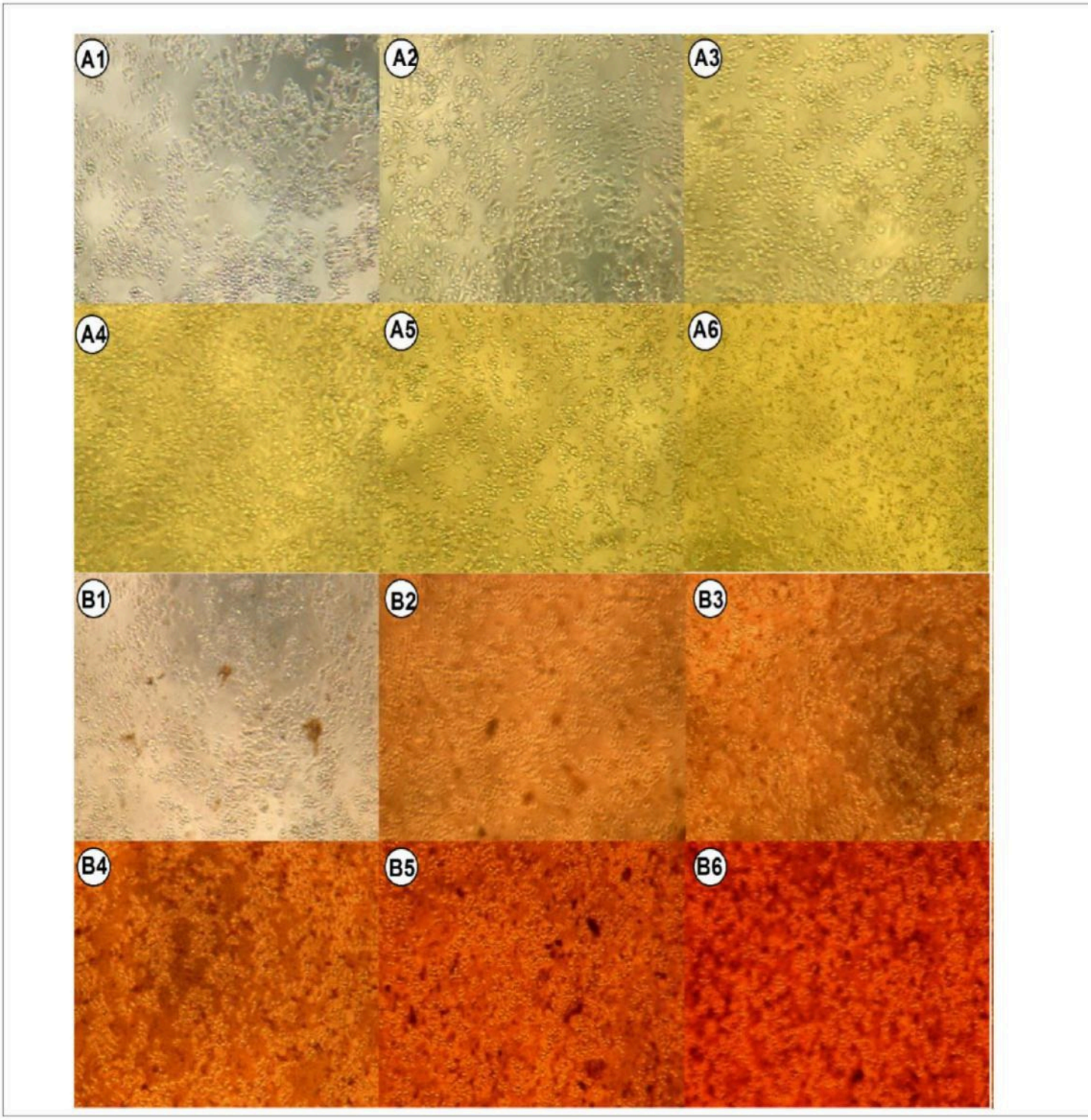


Figure 3

Optical microscopy images of HBE cells at 24 h after seeding. (A) Curcumin (A1) 0 μg/mL; (A2) 625 μg/mL; (A3) 937.5 μg/mL; (A4) 1,250 μg/mL; (A5) 1,875 μg/mL; (A6) 2,500 μg/mL; (B) Curcumin-Ag (B1) 2 μg/mL; (B2) 4 μg/mL; (B3) 10μg/mL; (B4) 25 μg/mL; (B5) 30 μg/mL; (B6) 50 μg/mL.

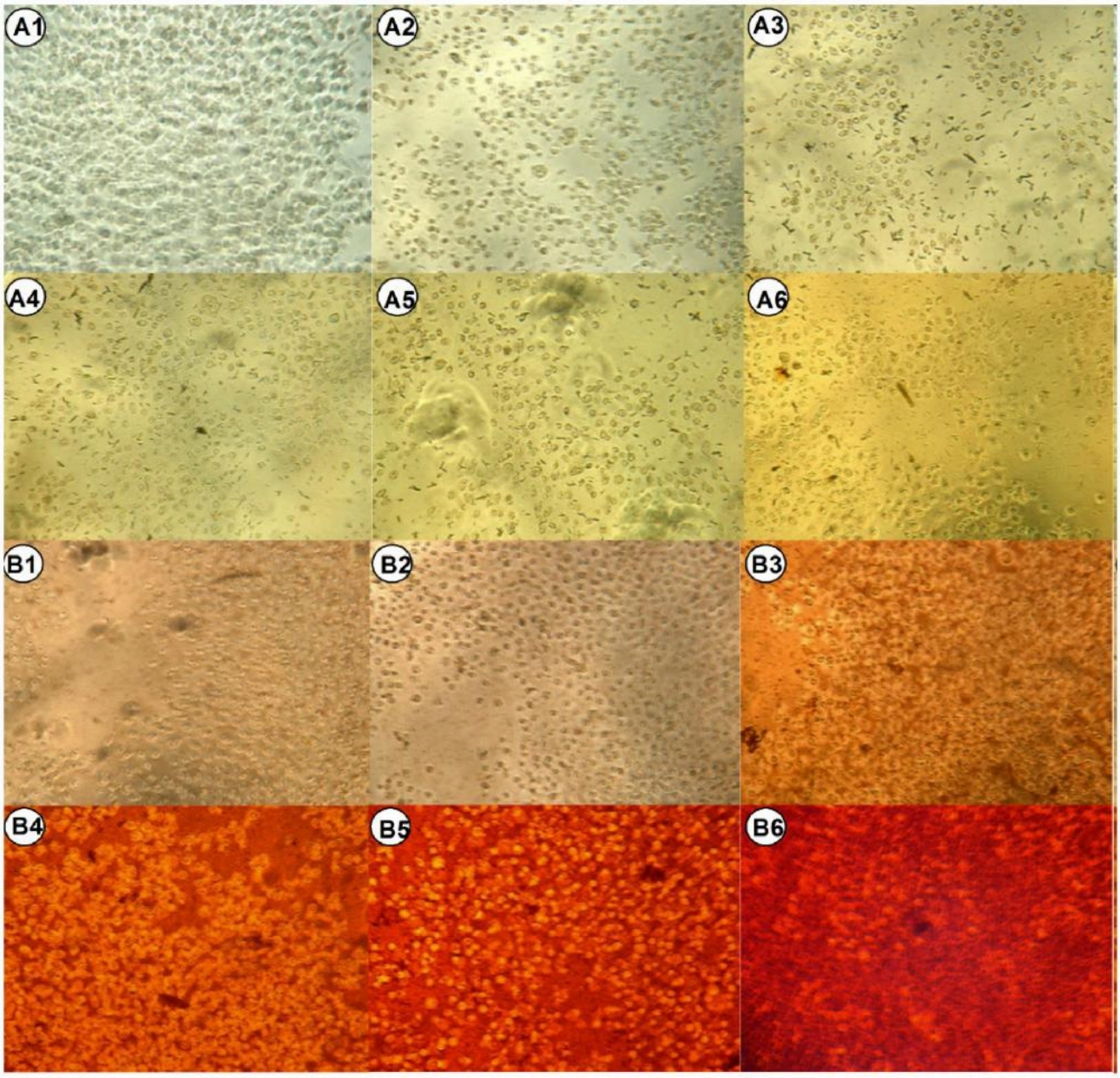


Figure 4

Optical microscopy images of HTB-182 cells at 24 h after seeding. (A) Curcumin (A1) 0 μg/mL; (A2) 625 μg/mL; (A3) 937.5 μg/mL; (A4) 1,250 μg/mL; (A5) 1,875μg/mL; (A6) 2,500 μg/mL (B) Curcumin-Ag; (B1) 2 μg/mL; (B2)4 μg/mL; (B3) 10 μg/mL; (B4) 25 μg/mL; (B5) 30 μg/mL; (B6) 50 μg/mL.

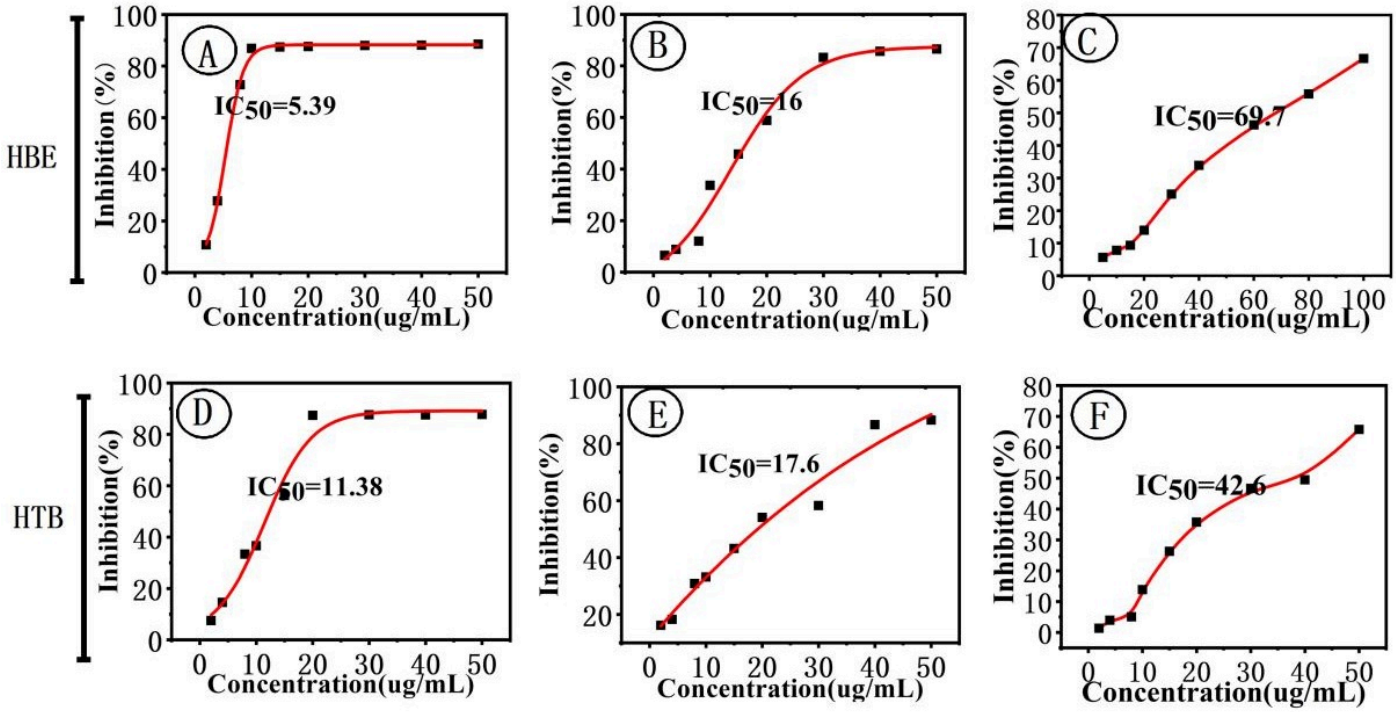


Figure 5

IC_{50} of Curcumin , Curcumin-AgNPs, and Ag+ on HBE and HTB cells.

(A)HBE-Ag+;(B)HBE-Curcumin-AgNPs;(C)HBE-Curcumin(D)HTB-Ag+(E)HTB-Curcumin-AgNPs.(F)HTB-Curcumin

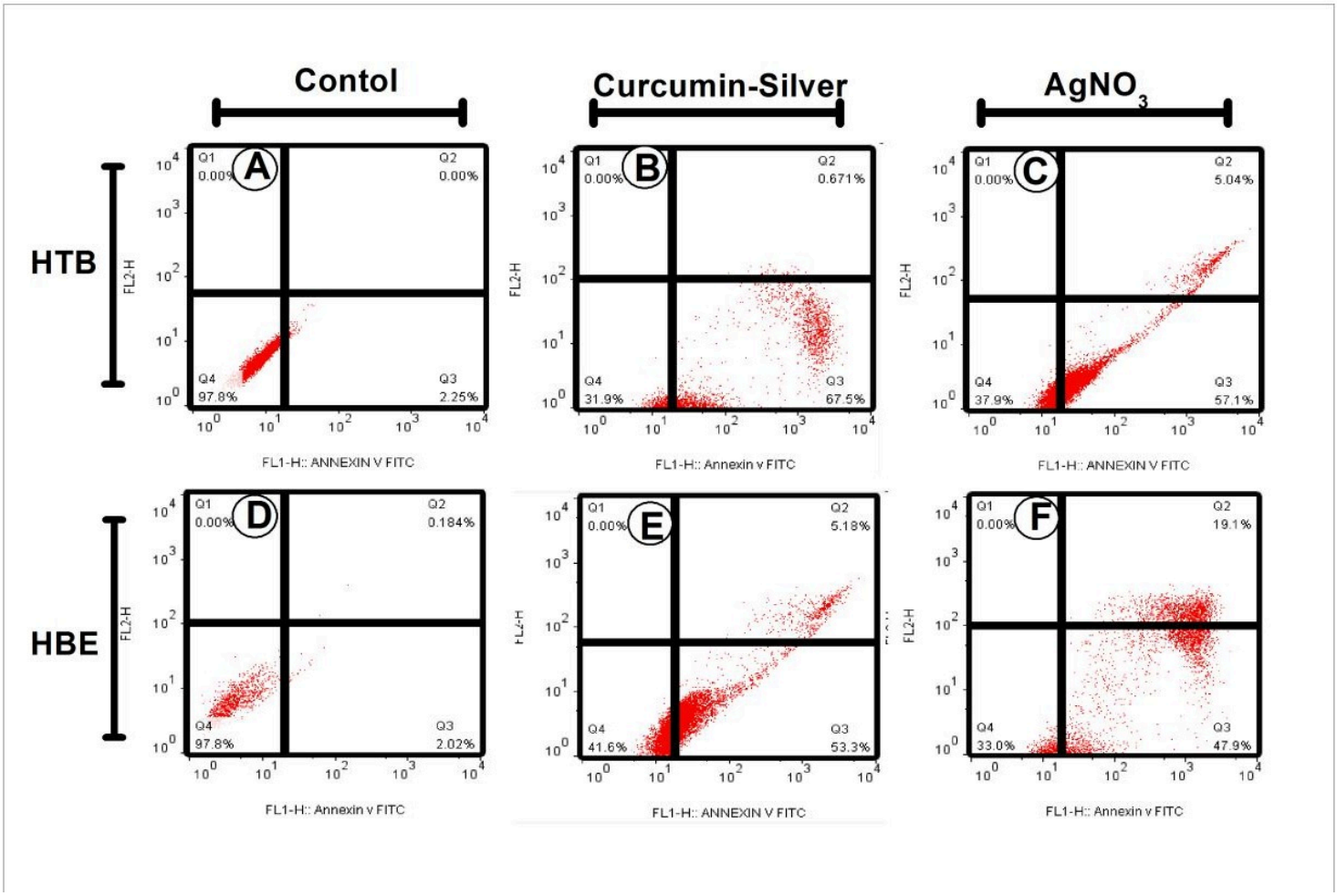


Figure 6

Flow cytometric analysis of FITC-annexin V-PI stained HBE and HTB-182 cells after AgNPs and Ag^+ treatment. Apoptotic and necrotic populations (%) in each sample were calculated from flow cytometric analysis. The values are represented as mean (SD) of three individual experiments. (A) HTB-Control; (B) HTB-Curcumin-AgNPs;(C)HTB-Ag+; (D) HBE-Control; (E) HBE-Curcumin-AgNPs; (F) HBE-Ag+. The concentrations of AgNPs and Ag^+ are 5 μg/mL, respectively.

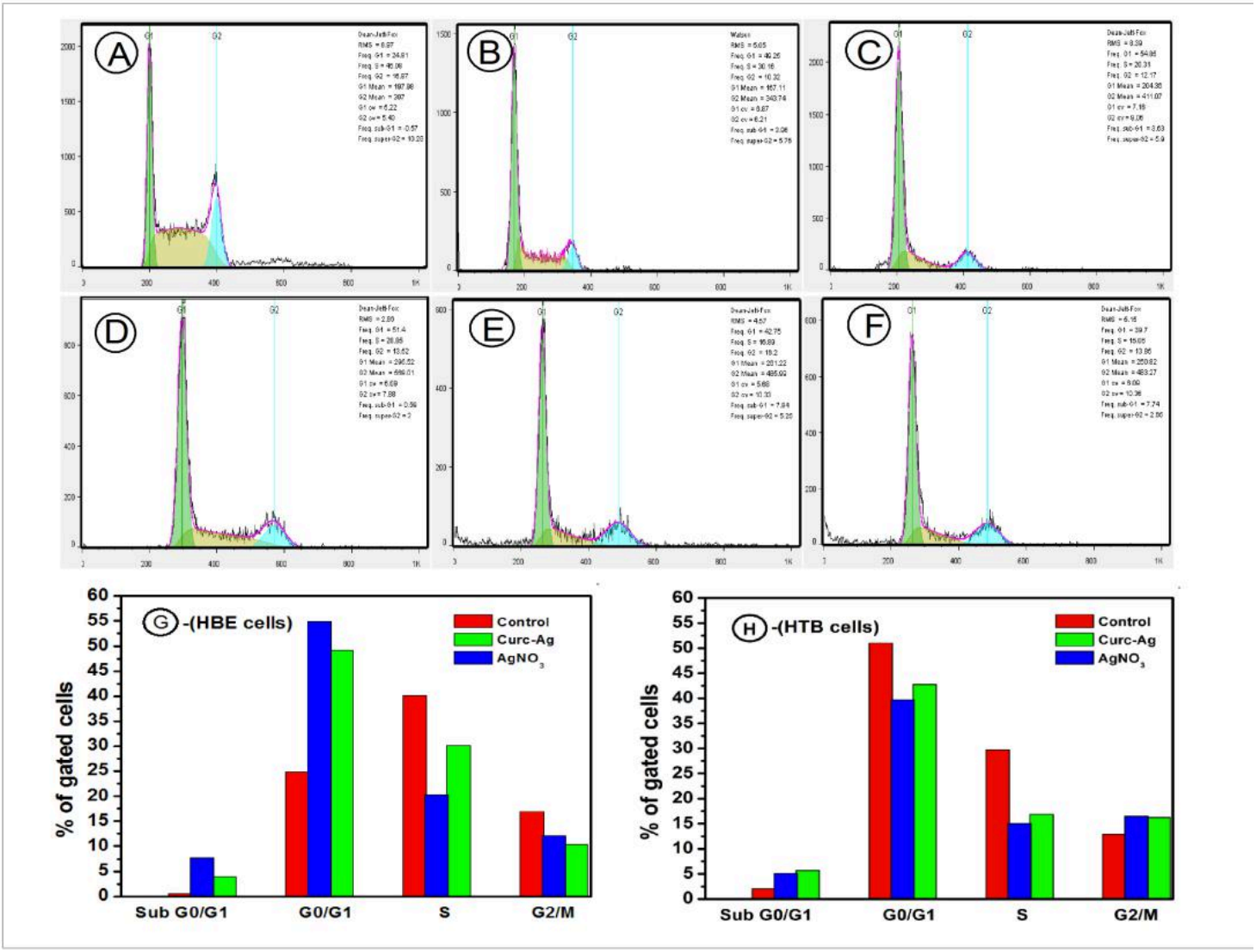


Figure 7

(A)-(H): Cell cycle analysis of HBE and HTB cells in the presence of AgNPs and $AgNO_3$ using flow cytometry.(A)HBE-Control;(B) HBE-Curcumin-AgNPs;(C) HBE-Ag^+; (D) HTB-Control; (E) HTB-Curcumin-AgNPs; (F) HTB-Ag^+; (G) and (H) Effect of AgNPs on cell cycle distribution evaluated by calculating the percentage of cells in each phase from flow cytometric data. The values are presented as the mean (SD) of three individual experiments. (G) HBE cells; (H) HTB cells; the concentration of AgNPs was 5 μg/mL.

Supplementary Files

This is a list of supplementary files associated with this preprint. Click to download.

- SC1.jpeg